Fine-structure electron-impact excitation of Ne+ and Ne2 + for low-temperature astrophysical plasmas

Monthly Notices
of the
ROYAL ASTRONOMICAL SOCIETY

MNRAS **469,** 1225–1232 (2017) doi:10.1093/mnras/stx553

Fine-structure electron-impact excitation of Ne^+ and Ne^{2+} for low-temperature astrophysical plasmas

Qianxia Wang,[1,2] S. D. Loch,[1]★ Y. Li,[1] M. S. Pindzola,[1] R. S. Cumbee,[3,4] P. C. Stancil,[3] B. M. McLaughlin[5] and C. P. Ballance[5]★

[1]*Department of Physics, Auburn University, Auburn, AL 36849, USA*
[2]*Department of Physics and Astronomy, Rice University, Houston, TX 77005, USA*
[3]*Department of Physics and Astronomy and Center for Simulational Physics, University of Georgia, Athens, GA 30602, USA*
[4]*NASA Goddard Space Flight Center, Greenbelt, MD 20771, USA*
[5]*Centre for Theoretical Atomic and Molecular Physics (CTAMOP), School of Mathematics and Physics, Queen's University Belfast, Belfast BT7 1NN, Northern Ireland*

Accepted 2017 March 2. Received 2017 February 10; in original form 2016 July 12

ABSTRACT

Collision strengths for the electron impact of the fine-structure levels within the ground term of Ne^+ and Ne^{2+} are calculated using the Breit–Pauli R-matrix and the Dirac atomic R-matrix code (DARC) methods. Maxwellian-averaged effective collision strengths are presented for each ion. The application of the current calculations is to very low temperature astrophysical plasmas, down to 10 K, and thus we examine the sensitivity of the effective collision strengths to the resonance positions and underlying atomic structure. The use of the various theoretical methods allows us to place estimated uncertainties on the recommended effective collision strengths. Good agreement is found with previous R-matrix calculations at higher temperatures.

Key words: atomic data – atomic processes.

1 INTRODUCTION

Electron-impact fine-structure excitation of low-charged ions is an important cooling mechanism in most interstellar environments, especially in regions with significant ionization fraction where electron-impact excitation is a strong populating mechanism for the excited states. The lines from these fine-structure transitions can be observed from the infrared (IR) to the submillimetre (submm) by a range of telescopes, such as the *Spitzer Space Telescope*, the Stratospheric Observatory for Infrared Astronomy (SOFIA), the *Herschel Space Observatory*, the Atacama Large Millimeter Array (ALMA), etc. Furthermore, fine-structure excitation due to electron impact is an important diagnostic tool for the density, pressure, temperature and/or ambient radiation field, if sufficiently accurate rate coefficients can be obtained. Electron-impact fine-structure excitation has been studied fairly extensively for many ions over the past few decades (Pradhan 1974; Saraph 1978; Butler & Mendoza 1984; Johnson, Burke & Kingston 1987; Saraph & Tully 1994; Griffin, Mitnik & Badnell 2001; Colgan et al. 2003; Berrington et al. 2005; Witthoeft, Whiteford & Badnell 2007; Munoz Burgos et al. 2009; Ludlow et al. 2011; McLaughlin et al. 2011; Malespin et al. 2011; Wu et al. 2012; Abdel-Naby et al. 2013, 2015) with R-matrix data being used in most modelling data bases. However, almost all of these studies have primarily focused on high energies/high temperatures relevant to collisionally ionized plasmas, and thus much of the low-temperature data being used has been extrapolated from the available R-matrix data. Also, there has been no detailed study on the uncertainty of the low-temperature rate coefficients. Thus, the aim of this paper is to produce a set of recommended fine-structure rate coefficients for the ground term of Ne^+ and Ne^{2+}, along with an estimated set of uncertainties.

For plasmas of importance in this paper, we require rate coefficients down to approximately 10 K; it should be noted that achieving accuracy in the underlying cross-section at this temperature is difficult. Therefore, it is important for astrophysical models that collisional calculations are performed of sufficient accuracy at lower energies for the low-temperature rate coefficients. This will extend the available data down to lower temperatures than exist currently in data bases and it will also improve the accuracy of the low-temperature rate coefficients.

The fine-structure line emissions from Ne II and Ne III, populated via electron-impact excitation, are observed in the IR and are known to be very important for probing H II regions. Previous work (Glassgold, Najita & Igea 2007; Meijerink, Glassgold & Najita 2008) proposed that Ne II and Ne III fine-structure lines could serve as a diagnostic of the source of an evaporative flow, as well as of signatures of X-ray irradiation, the so-called X-ray dominated regions (XDRs). This is because hard X-rays have sufficient energy to generate multiple ionization states of neon, which can then be collisionally excited. R-matrix calculations have been available for these and neighbouring ion stages of Ne. Specifically, collision strengths

★ E-mail: loch@physics.auburn.edu (SDL); C.Ballance@qub.ac.uk (CPB)

for the $1s^2 2s^2 2p^5$ ($^2P^0_{3/2}$)–($^2P^0_{1/2}$) transition of Ne^+ have been calculated using an R-matrix method via the JAJOM approach (Saraph 1978; Johnson et al. 1987; Saraph & Tully 1994), which transforms *LS*-coupled K-matrices into level–level cross-sections. The collision strengths of the transitions among levels of the lowest configurations for Ne^{2+} were evaluated by Pradhan (1974) and Butler & Mendoza (1984) using the IMPACT close-coupling code. McLaughlin & Bell (2000), McLaughlin, Daw & Bell (2002) and McLaughlin et al. (2011) extended this approach to a large configuration-interaction (CI) representation of the target, supplemented by a few extra pseudo-orbitals to improve the target description further.

Here, we have re-investigated these two Ne ions for several reasons. Previous work has focused primarily on higher electron-impact energies than considered here, with only a few of their Maxwellian-averaged effective collision strengths going below 800 K. Thus, we investigate the sensitivity of the very low-temperature rate coefficients to changes in the atomic structure, threshold energies and resonance positions. This leads naturally to the second focus of the paper, which is the exploration of uncertainty in the rate coefficients at very low temperatures. To this end, two different theoretical level-resolved R-matrix approaches have been applied: the Breit–Pauli (BP) approximation (Berrington 1987) and the fully relativistic Dirac method (Norrington & Grant 1981; Dyall et al. 1989; Grant 2007). Ostensibly, if the underlying electronic structure adopted in each approach was exactly the same, then there would be little expectation of differences in the collision strengths. However, with the use of different atomic structure codes and the choices made in their use, this invariably leads to small differences in transition probabilities (Einstein *A* coefficients) and, subsequently, dynamical quantities such as collision strengths.

Because of the low-temperature focus of this paper, we are interested in the sensitivity of the effective collision strengths to the threshold energy position, the target wavefunctions, resonance positions and anything that can affect the background cross-section. We appreciate that the height and position of a single resonance can dramatically affect the results at these temperatures. We shall explore the variation in results to threshold energy and resonance positions by calculating collision strengths where the target energies have been shifted (or not) to National Institute of Standards and Technology (NIST) energies (Kramida et al. 2015). Furthermore, we explore the sensitivity of the target wavefunction via different target expansions within the BP R-matrix and Dirac atomic R-matrix code (DARC) methods. After investigating the differences between all calculated effective collision strengths for the same transition, a recommended data set is determined for each ion.

We focus on excitation at low temperatures (10–2000 K) in this paper. So, for Ne^+, only rates for the transition between the two lowest levels $1s^2 2s^2 2p^5$ ($^2P^0_{3/2}$)–($^2P^0_{1/2}$) are presented. Also, the transitions between the three lowest fine-structure levels of Ne^{2+} (see the energy diagram in Fig. 1) are investigated here.

The rest of this paper is organized as follows. In Section 2, we describe the theoretical methods used in this paper, and in Section 3, we present the details of the calculations. We discuss the calculated results, target energies, Einstein *A* coefficients, collision strengths and effective collision strengths for Ne^+ and Ne^{2+} in Section 4. In Section 5, we provide a summary of the results.

2 THEORY

Level-resolved electron-impact excitation cross-section calculations, using R-matrix theory, employ a similar formalism either

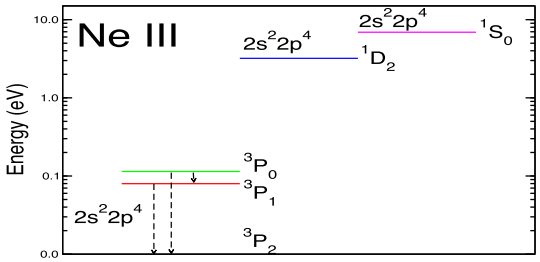

Figure 1. Energy diagram for Ne III. Three fine-structure transitions are shown: $2s^2 2p^4$ ($^3P_1$)–($^3P_2$), $2s^2 2p^4$ ($^3P_0$)–($^3P_1$) and $2s^2 2p^4$ ($^3P_0$)–($^3P_2$).

in semirelativistic (BP) or relativistic (DARC) implementations. Ne^+ and Ne^{2+} are not highly charged, and therefore both semirelativistic and fully relativistic methods are equally applicable. The main differences arise from the choices made in the determination of the target orbitals for use in dynamical calculations. The atomic structure code AUTOSTRUCTURE (Badnell 1986) generates non-relativistic orbitals whereas the general relativistic atomic structure package (GRASP; Dyall et al. 1989; Grant 2007) formulates and diagonalizes a Dirac–Coulomb Hamiltonian to produce the relativistic orbitals. The former is used in the BP/intermediate-coupling frame transformation (ICFT; Berrington, Eissner & Norrington 1995; Griffin, Badnell & Pindzola 1998) R-matrix collisional calculations and the latter in the DARC (Chang 1975; Norrington & Grant 1981; Grant 2007) calculations to obtain level-to-level electron-impact excitation cross-sections.

The BP R-matrix method is a set of parallel codes developed from modified serial versions of the RMATRX I codes (Berrington et al. 1995). Both the BP and ICFT models recouple underlying *LS*-coupling calculations; the former transforms several *LS*-resolved Hamiltonians into a *jK*-coupled Hamiltonian, as opposed to the ICFT approach that transforms unphysical *LS*-resolved K-matrices into level-resolved collision strengths. In general, there has been very good agreement between the ICFT and BP R-matrix methods (Griffin et al. 1998; Munoz Burgos et al. 2009; McLaughlin et al. 2011).

The implementation of various flavours of R-matrix theory are used in this study. The review book of Burke (2011) provides an excellent overview of non-relativistic (*LS* coupling), semirelativistic (BP/ICFT) and relativistic (DARC) electron-impact excitation. The comparison of BP and ICFT results benefits from the use of a completely consistent atomic structure calculation. Thus, the comparison with the multiconfiguration Dirac–Fock (MCDF) structure results from GRASP and the resulting DARC collision strengths provides a means to investigate effects due to changes in the target structure. In all cases, every effort has been made to optimize the orbitals on the fine-structure levels of the ground term. The DARC calculation employs relativistic orbitals from the initial atomic structure calculations throughout the remainder of the computation. It should be restated that low-temperature astrophysical constraints on both our Ne systems means we are pursuing only transitions between the fine-structure levels of the ground term, and that any excited states are included for the main purpose of improving the energy levels of those low-lying states through configuration interaction. Given that the energy separation between the ground state $n = 2$ and the excited $n = 3$ levels for either Ne^+ or Ne^{2+} exceeds 2 Ry, it is unlikely that Rydberg states attached to the $n = 3$ levels would perturb our $n = 2$ results.

Table 1. Target expansions for Ne^+ and Ne^{2+}.

Ne^+ DARC/BP $n=2$	Ne^+ DARC/BP $n=3$	Ne^{2+} DARC/BP $n=2$	Ne^{2+} DARC/BP $n=3$
$1s^22s^22p^5$	$1s^22s^22p^5$	$1s^22s^22p^4$	$1s^22s^22p^4$
$1s^22s2p^6$	$1s^22s2p^6$	$1s^22p^6$	$1s^22p^6$
	$1s^22s2p^53l$	$1s^22s2p^5$	$1s^22s2p^5$
	$1s^22s^22p^43l$		$1s^22s2p^43l$
			$1s^22s^22p^33l$
			$1s^22p^53l$

Table 2. Scattering calculation parameters used in our work on Ne II and Ne III ions for different target expansions.

	Ne II $n=2$	Ne II $n=3$	Ne III $n=2$	Ne III $n=3$
Radius of R-matrix sphere (au) (DARC, BP)	5.40, 5.87	19.83, 21.60	4.89,5.24	13.28, 14.35
Continuum basis orbitals for each angular momentum	20	20	20	20
Partial waves J	0–20	0–20	0–20	0–20
Energy mesh (Ry)	2.5×10^{-6}	2.5×10^{-6}	3.125×10^{-6}	3.125×10^{-6}
Energy range (Ry)	0.007–0.107	0.007–0.107	0.0058–0.1658	0.0058–0.1658
Temperature range (K)	10–2000	10–2000	10–2000	10–2000

3 CALCULATION DETAILS

3.1 Target-state calculation

Given the low-temperature focus of this paper, only small-scale calculations are required for the fine-structure transitions within the ground term. Furthermore, we explore the variation of our results in relation to various CI expansions. Thus, we consider both a small and larger CI expansion for Ne^+ and Ne^{2+}, with the configurations described in Table 1. The models are referred to as BP $n=2$, DARC $n=2$, BP $n=3$ and DARC $n=3$.

Orbitals are optimized automatically using the GRASP code (Dyall et al. 1989; Grant 2007), which are then used in subsequent scattering calculations within the Dirac R-matrix method. We focus on low energies, and the orbitals of interest belong then to the first several terms. Scattering calculations for the DARC $n=3$ model use orbitals obtained from GRASP from the DARC $n=2$ model, which are held fixed. This improves the energies and A-values of the levels in the ground term. We note that if all orbitals are optimized simultaneously in a GRASP $n=3$ calculation, then this leads to much larger differences with NIST values. Thus, our GRASP $n=2$ and $n=3$ calculations for both ions are optimized for the fine-structure levels of interest to this work. In the GRASP calculations for each ion, we used the option of extended average level (EAL) to optimize the energies.

For the BP scattering models, we optimize the target input orbitals using AUTOSTRUCTURE (Badnell 1986) with different sets of parameters. We developed a code to vary the orbital scaling parameters used in AUTOSTRUCTURE, comparing the resulting energies and A-values with NIST values until a minimum was found in the differences (for the transitions of interest) with the NIST tabulated values (Kramida et al. 2015). The optimized orbital scaling parameters are as follows: $\lambda_{1s}=0.8$, $\lambda_{2s}=1.2$ and $\lambda_{2p}=1.08$ for BP $n=2$ calculations of Ne III; $\lambda_{1s}=0.8$, $\lambda_{2s}=1.2$, $\lambda_{2p}=1.08$, $\lambda_{3s}=0.8$, $\lambda_{3p}=1.2$ and $\lambda_{3d}=0.8$ for BP $n=3$ calculations of Ne III.

Similarly, we use the same procedure to generate parameters for the target orbitals for Ne II BP $n=2$ and $n=3$ collision models. However, in this case, we find that the resulting effective collision strengths do not change much compared with the unoptimized structure results, and therefore we adopted the unoptimized parameters for the target orbitals in our BP collision calculations for Ne^+ in this paper. It should be noted that these BP results for Ne II will not be used for our recommended data, and instead will be used only in estimating the uncertainty on our final data.

3.2 Scattering calculation

Details specific to the current R-matrix calculations are summarized in Table 2, where we have included all the relevant parameters used in the different calculations. The radius of the R-matrix sphere for the different collision calculations is selected automatically during the R-matrix calculations. The numbers of continuum basis orbitals for each angular momentum and numbers of partial waves are chosen to converge with the results for the low-temperature calculations. The energy mesh is selected to ensure resonances were fully resolved, particularly for the lowest temperatures and the subsequent effective collision strengths. The energy ranges calculated for the collision strengths are determined by the temperature range of interest for the effective collision strengths. It should also be noted that all of the energy levels in the target structure calculations were included in the scattering calculations.

3.3 Effective collision strength calculation

The effective collision strength (Seaton 1953; Eissner et al. 1969) can be calculated from the collision strengths using

$$\Upsilon_{ij} = \int_0^\infty \Omega_{ij} \exp\left(\frac{-\epsilon_j}{kT_e}\right) \mathrm{d}\left(\frac{\epsilon_j}{kT_e}\right), \quad (1)$$

where Ω_{ij} is the collision strength for the transition from level i to j, ϵ_j is the energy of the scattered electron, T_e is the electron temperature and k is the Boltzmann constant.

The Maxwellian excitation rate coefficient, q_{ij}, is used widely in astrophysical modelling codes. The relationship between q_{ij} and Υ_{ij} is

$$q_{ij} = 2\sqrt{\pi}\alpha c a_0^2 \left(\frac{I_H}{kT_e}\right)^{1/2} \frac{1}{\omega_i} \mathrm{e}^{-(\Delta E_{ij}/kT_e)} \Upsilon_{ij}, \quad (2)$$

where α is the fine-structure constant, c is the speed of light, a_0 is the Bohr radius, I_H is the hydrogen ionization potential, ΔE_{ij}

Table 3. Fine-structure energy levels for Ne II and Ne III (in Ry) compared to the NIST values (Kramida et al. 2015). The configurations and terms listed in the first two columns label different levels. Column 3 gives the corresponding energies from the tabulated NIST values. The percentage error after each theoretical energy indicates the deviation from the NIST value. The last line for each ion in the table is the average error $\delta\%$ of each theoretical calculation.

Configuration	Term ($^{2s+1}L_J$)	NIST	BP $n=2$	$\delta\%$	BP $n=3$	$\delta\%$	DARC $n=2$	$\delta\%$	DARC $n=3$	$\delta\%$
Ne II $2s^22p^5$	$^2P^0_{3/2}$	0.0000	0.0000	0	0.0000	0	0.0000	0	0.0000	0
	$^2P^0_{1/2}$	0.0071	0.0069	2.82	0.0070	1.91	0.0076	7.2	0.0079	11.3
Avg. $\delta\%$				1.41		0.96		3.6		5.65
Ne III $2s^22p^4$	$^3P_2$	0.0000	0.0000	0	0.0000	0	0.0000	0	0.0000	0
	$^3P_1$	0.0059	0.0057	3.39	0.0057	3.39	0.0060	1.59	0.0061	3.39
	$^3P_0$	0.0084	0.0084	0	0.0083	1.19	0.0088	4.33	0.0090	7.14
	$^1D_2$	0.2355	0.2513	6.70	0.2557	8.58	0.2521	7.05	0.2470	4.88
	$^1S_0$	0.5081	0.4942	2.76	0.4914	3.29	0.4795	5.62	0.4734	6.83
Avg. $\delta\%$				2.57		3.29		3.72		4.45

Table 4. Einstein A coefficients (in s^{-1}) for magnetic-dipole transitions (M1), within the same configuration, for the Ne II and Ne III ions compared to the NIST values (Kramida et al. 2015). Columns are as in Table 3.

	NIST	BP $n=2$	$\delta\%$	BP $n=3$	$\delta\%$	DARC $n=2$	$\delta\%$	DARC $n=3$	$\delta\%$
Ne II									
$2s^22p^5$ ($^2P^0_{3/2}$)–($^2P^0_{1/2}$)	8.59×10^{-3}	7.84×10^{-3}	8.68	8.07×10^{-3}	6.1	8.16×10^{-3}	5.01	8.14×10^{-3}	5.24
Ne III									
$2s^22p^4$ ($^3P_2$)–($^3P_1$)	5.84×10^{-3}	5.47×10^{-3}	6.34	5.42×10^{-3}	7.19	5.86×10^{-3}	0.42	5.81×10^{-3}	0.51
$2s^22p^4$ ($^3P_1$)–($^3P_0$)	1.10×10^{-3}	1.38×10^{-3}	25.45	1.36×10^{-3}	23.64	1.15×10^{-3}	4.95	1.14×10^{-3}	3.64
Avg. $\delta\%$			15.90		15.42		2.69		2.08

is the energy difference in the fine-structure levels and ω_i is the degeneracy in the lower level. Compared with $q_{ij}(T_e)$, $\Upsilon_{ij}(T_e)$ is a smoother function and can be more accurately interpolated.

4 RESULTS AND DISCUSSION

Astrophysical plasma modellers who study IR/submm observations of low-temperature plasmas, such as the interstellar medium, require atomic rate coefficients down to temperatures as low as 10 K. This places very stringent tests on the accuracy of the atomic structure and collisional calculations. The excitation rate coefficients will be very sensitive to small changes in the atomic structure. As a result, the structure will affect the rate coefficients through changes in the threshold energy, resonance strengths and positions, and changes in the background cross-section. For this reason, we have performed a range of calculations using different methods (BP $n=2$, DARC $n=2$, BP $n=3$ and DARC $n=3$). These methods are used to explore the variation of the effective collision strengths, particularly at low temperatures. The purpose of including the $n=3$ configurations is to improve the energies and transition probabilities for the levels within the ground term.

4.1 Bound-state energies and radiative rates for Ne^+ and Ne^{2+}

Our recommended data set shall be the model that minimizes the difference between the calculations and NIST A-values and level energies (Kramida et al. 2015). The results are shown in Tables 3 and 4. The percentage error ($\delta\%$) shown is calculated by $[(x - x_{\rm NIST})/x_{\rm NIST}] \times 100$ per cent with the NIST data providing the accepted values.

AUTOSTRUCTURE (Badnell 1986) and GRASP (Dyall et al. 1989; Grant 2007) are two different atomic strucuture codes used to generate target energies and orbitals for the BP and DARC R-matrix methods, respectively. They give rise to 3 and 108 levels for Ne^+, and 10 and 226 levels for Ne^{2+} for $n=2$ and $n=3$ target expansions. The energies for the levels within the ground term are presented in Table 3 and the associated A-values in Table 4. In general, the percentage errors show that the agreement between theoretical and NIST values is reasonable. For Ne^+, the average percentage error for the BP $n=2$, BP $n=3$, DARC $n=2$ and DARC $n=3$ target expansions are 1.41, 0.96, 3.6 and 5.65 per cent, respectively. For Ne^{2+}, the corresponding average percentage errors for target energies are 2.57, 3.29, 3.72 and 4.45 per cent.

Table 4 presents the comparison of Einstein A coefficients of the magnetic-dipole (M1) for both the Ne^+ and Ne^{2+} transitions. Because of the reasonable agreement for all the calculations with NIST energies, we use the A-values as our main selection criteria in recommending a final data set for Ne^+ and Ne^{2+}. In both cases, the GRASP code produces closer agreement with NIST A-values, compared with AUTOSTRUCTURE. The accuracy of the Einstein A coefficient depends on both the precision of the target energies and the reliability of the target wavefunctions. The A-values produced by GRASP $n=2$ and $n=3$ are close, because they use the same orbitals. Overall, the $n=2$ GRASP calculation has slightly better agreement with NIST A-values and energies than the GRASP $n=3$ calculation; thus, our recommended data set for both ions is the DARC $n=2$ calculation. The other calculations can be used to gauge the variation between the different calculations, and will be used to produce an uncertainty estimate on our recommended data.

4.2 Collision strengths and effective collision strengths for Ne^+ and Ne^{2+}

To our knowledge, there are no experimental results for the collision strengths for transitions within the ground complex for either of these ion stages. Our goal is to determine the variation in effective collision strengths between our best models as we progress to the very low temperatures required by the astrophysical applications.

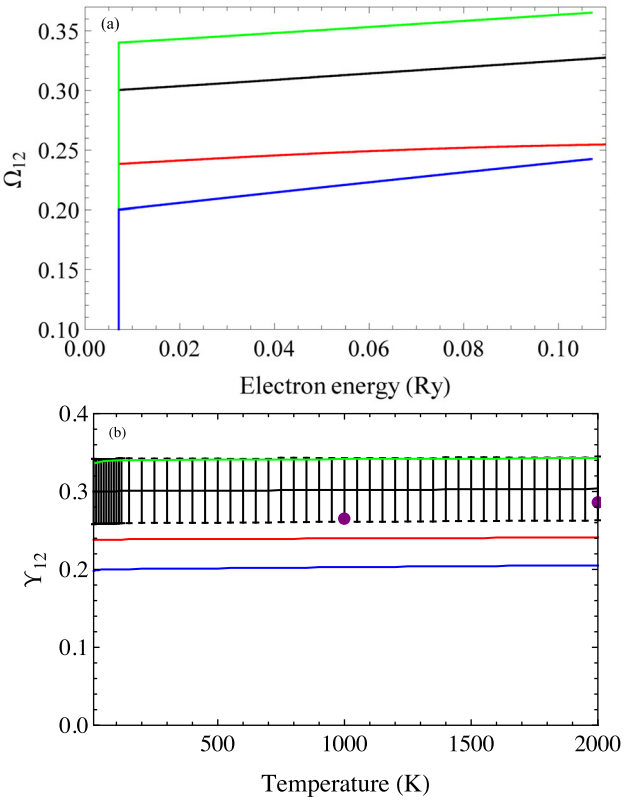

Figure 2. Comparison of Ne II collision strengths (a) and effective collision strengths (b) for the $2s^2 2p^5$ ($^2P^0_{3/2}$)–($^2P^0_{1/2}$) transition between different target expansions: DARC $n = 2$ (black line), DARC $n = 3$ (red line), BP $n = 2$ (green line) and BP $n = 3$ (blue line). Uncertainty estimates are given for our recommended DARC $n = 2$ results together with a comparison with the previous R-matrix calculation (purple circles) (Griffin et al. 2001).

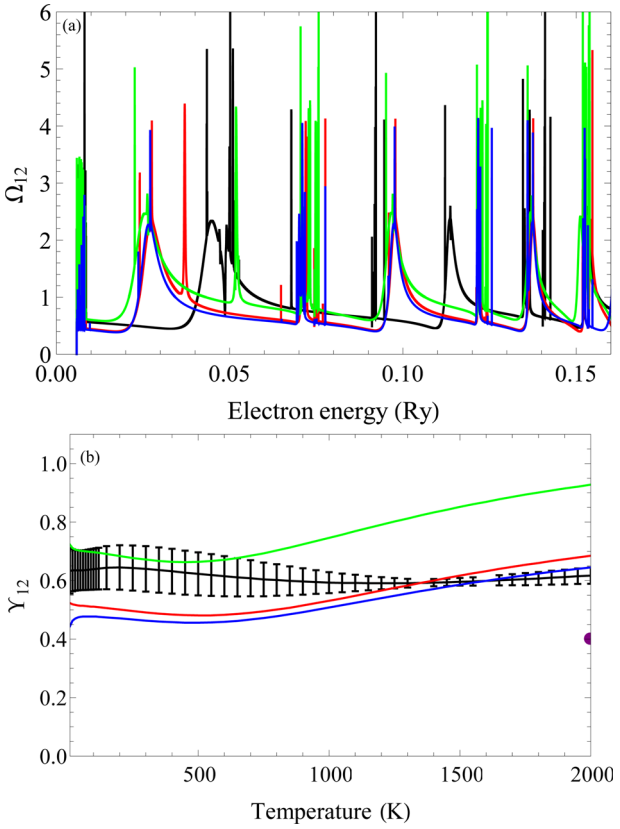

Figure 3. Comparison of Ne III collision strengths (a) and effective collision strengths (b) for the $2s^2 2p^4$ ($^3P_2$)–($^3P_1$) transition between different target expansions: DARC $n = 2$ (black line), DARC $n = 3$ (red line), BP $n = 2$ (green line) and BP $n = 3$ (blue line). Uncertainty estimates are given for our recommended DARC $n = 2$ results together with a comparison with the previous R-matrix calculation (purple circle) (McLaughlin et al. 2011).

As stated above, the DIRAC $n = 2$ effective collision strengths will be our recommended data, with the some of the other calculations being used to provide an uncertainty estimate. We have considered two different approaches to calculating meaningful representative uncertainties in our work.

In the first approach, we calculate a percentage uncertainty on the effective collision strengths simply using the standard deviation of our three most accurate models as determined from the accuracy of the energy levels and the associated A-values, given by

$$\%\Delta = \frac{\sigma(\bar{x}_{\rm best})}{x_i} \times 100 \text{ percent}, \quad (3)$$

where $\sigma(\bar{x}_{\rm best})$ is the standard deviation. Then, in the second approach, we obtain a percentage difference comparing results from our semirelativistic and fully relativistic R-matrix methods, employing exactly the same set of non-relativistic target configurations. In this case, the percentage difference is calculated by

$$\frac{x_1 - x_2}{(x_1 + x_2)/2} \times 100 \text{ percent}.$$

Figs 2–5 illustrate the collision strengths and effective collision strengths for the fine-structure transitions of both Ne^+ and Ne^{2+}, using the different R-matrix methods. In the evaluation of these effective collision strengths, we use only our best calculations (i.e. optimized λ where possible and with threshold energies shifted to NIST values). It is, however, interesting to investigate the effect of shifting to NIST energies on the effective collision strengths. Thus, Figs 6–8 explore the effects of shifting the target threshold energies to NIST values using the BP $n = 3$ calculation for Ne^{2+}.

Sampling a range of calculations allows us to more objectively explore the variation of collision strength with regards to the size of the different CI expansions. As stated earlier, the sizeable energy separation between the $n = 2$ and $n = 3$ levels precludes the possibility of interloping resonances attached to the $n = 3$ levels perturbing the cross-sections from transitions amongst the $n = 2$ levels. The influence of resonance contributions to effective collision strengths is only expected for the case of Ne^{2+} because of the $2p^4$ subshell supporting three levels within the ground term, whereas the resonances attached to the upper $J = 1/2$ levels of $Ne^+(2p^5)$ lie in the elastic cross-section of the Ne^+ ground state.

Fig. 2 shows collision strengths (top) and effective collision strengths (bottom) for the Ne^+ $2s^2 2p^5$($^2P^0_{3/2}$)–($^2P^0_{1/2}$) transition. The largest collision strengths are from the BP $n = 2$ calculation, followed by the next lower DARC $n = 2$ calculation, and then DARC $n = 3$ and BP $n = 3$. The DARC $n = 2$ calculation is our recommended data set based upon A-value comparisons with the NIST values (Kramida et al. 2015). Furthermore, in the absence of experiments, the MCDF approach would be our recommended theoretical model. Subsequent effective collision strengths were generated from the respective collision strengths of each calculation. We note that beyond the current work, a previous large-scale BP R-matrix calculation for Ne^+ has been carried out by Griffin et al. (2001). However, the focus of that work was to provide a large

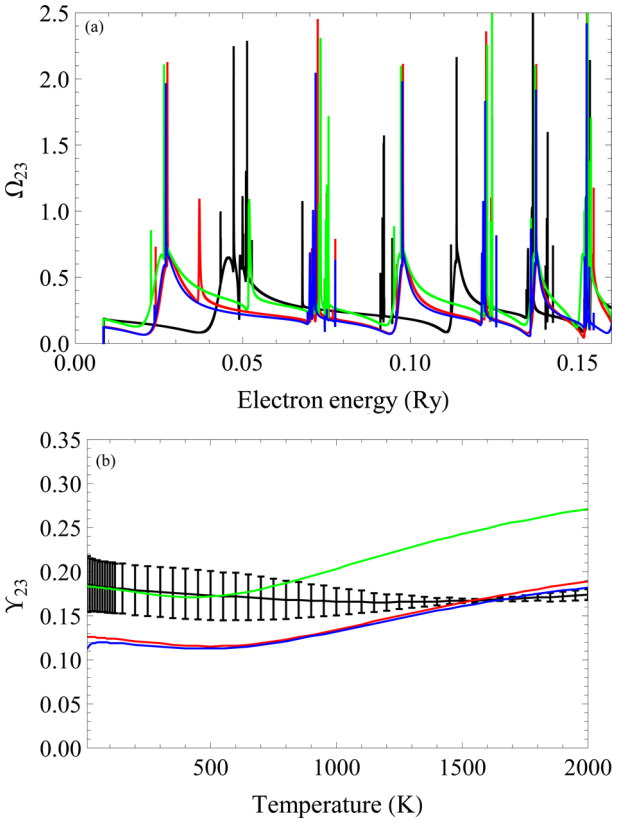

Figure 4. Comparison of Ne III collision strengths (a) and effective collision strengths (b) for the $2s^22p^4$ ($^3P_1$)–($^3P_0$) transition between different target expansions: DARC $n = 2$ (black line), DARC $n = 3$ (red line), BP $n = 2$ (green line) and BP $n = 3$ (blue line). Uncertainty estimates are given for our recommended DARC $n = 2$ results.

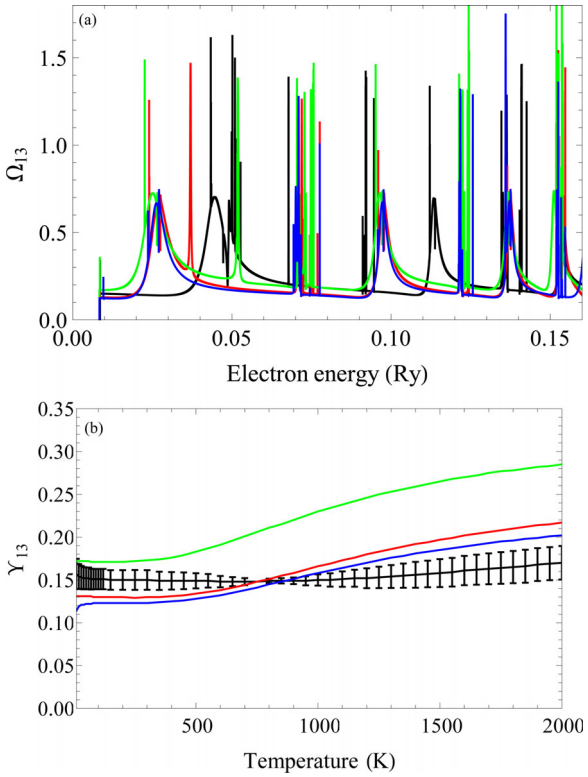

Figure 5. Comparison of Ne III collision strengths (a) effective collision strengths (b) for the $2s^22p^4$ ($^3P_2$)–($^3P_0$) transition between different target expansions: DARC $n = 2$ (black line), DARC $n = 3$ (red line), BP $n = 2$ (green line) and BP $n = 3$ (blue line). Uncertainty estimates are given for our recommended DARC $n = 2$ results.

comprehensive data set across a wide range of temperatures, but not at the very low temperatures required by our study. At 1000 and 2000 K, the DARC $n = 2$ effective collision strengths are in reasonable agreement with this previous work. Our effective collision strengths are 0.302 at 1000 K and 0.304 at 2000 K, compared with 0.266 and 0.286 from Griffin et al. (2001), as shown in Fig. 2, giving differences of 12.7 and 6.1 per cent, respectively. Thus, this supports our independent conclusion that our DARC $n = 2$ effective collision strengths should be the recommended data set at even lower temperatures. The recommended effective collision strengths are given in Table 5. These results can also be obtained in the formats of the Leiden Atomic and Molecular Database (LAMDA; Schöier et al. 2005) and the Stout data base (Lykins et al. 2015).

Employing the average percentage uncertainty given by equation (3), the $\bar{x}_{\rm best}$ values used to calculate the uncertainty are the BP $n = 3$, the DARC $n = 2$ and $n = 3$ results, providing an uncertainty of 13–14 per cent for our recommended DARC $n = 2$ effective collision strengths, as shown in Fig. 2.

It is also of interest to consider the differences between the DARC and BP calculations, for the cases when they both have the same configurations. The differences of the effective collision strengths between the DARC $n = 2$ and BP $n = 2$ are 11–13 per cent, while the DARC $n = 3$ and BP $n = 3$ differ by 16–18 per cent.

Considering next Ne^{2+}, Figs 3–5 present the collision strengths (top) and effective collision strengths (bottom) for three different transitions within the ground term, namely, the ($^3P_2$)–($^3P_1$) (Fig. 3), ($^3P_1$)–($^3P_0$) (Fig. 4) and ($^3P_2$)–($^3P_0$) (Fig. 5) transitions. The

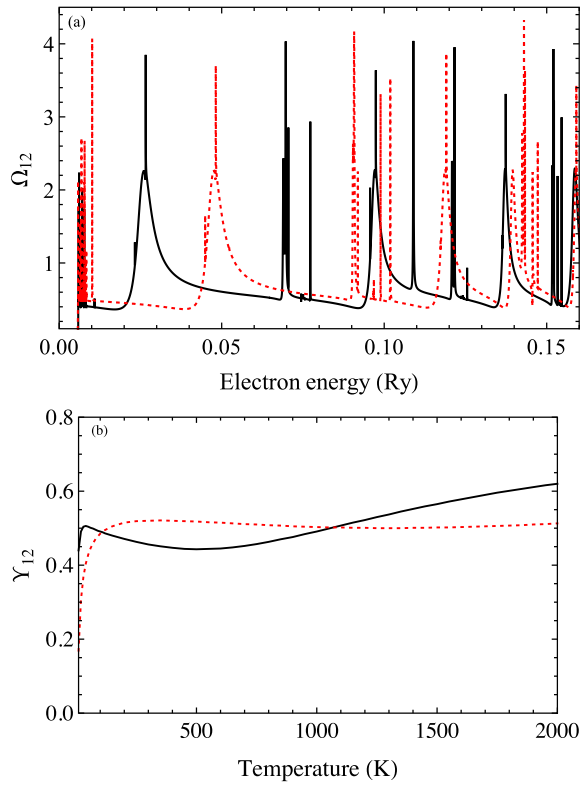

Figure 6. Comparison of Ne III collision strengths (a) and effective collision strengths (b) for the $2s^22p^4$ ($^3P_2$)–($^3P_1$) transition: BP $n = 3$ with (black solid line) and without (red dotted line) the energy shift.

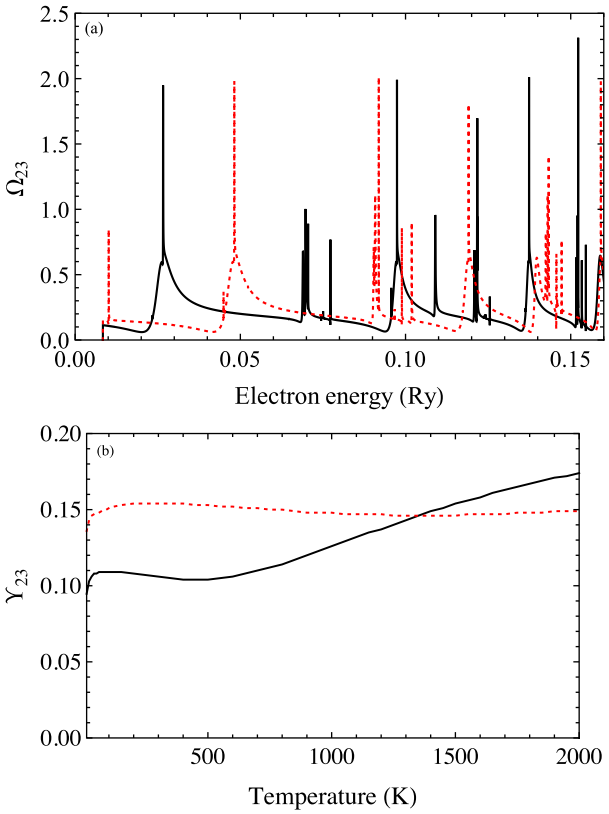

Figure 7. Comparison of the Ne III collision strengths (a) and effective collision strengths (b) for the $2s^22p^4$ ($^3P_1$)–($^3P_0$) transition: BP $n = 3$ with (black solid line) and without (red dotted line) the energy shift.

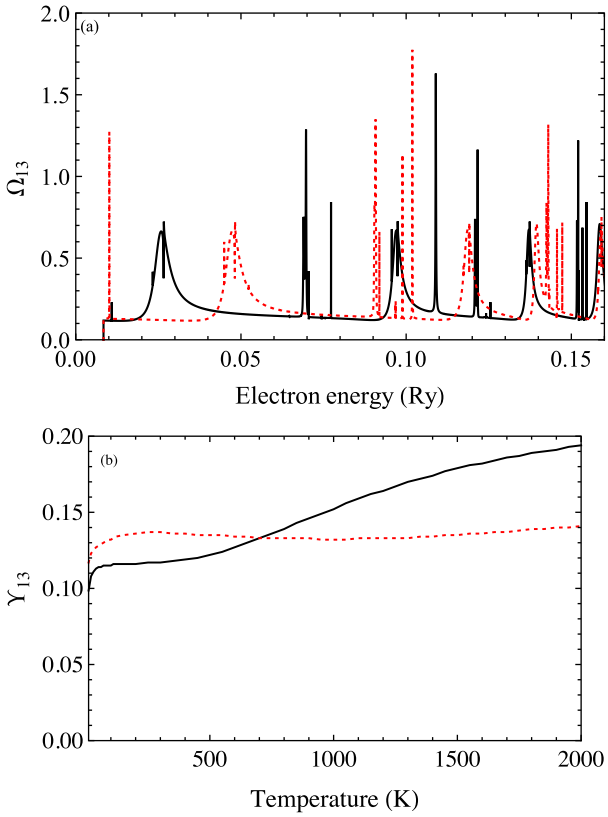

Figure 8. Comparison of Ne III collision strengths (a) and effective collision strengths (b) for the $2s^22p^4$ ($^3P_2$)–($^3P_0$) transition: BP $n = 3$ with (black solid line) and without (red dotted line) the energy shift.

collision strengths of different calculations have similar backgrounds for each of these transitions. However, the resonance positions are shifted for each calculation, which cause the observed difference in the effective collision strengths. Previous calculations by McLaughlin et al. (2011), which extended down to 2000 K, appear to be consistent with our recommended data, the DARC $n = 2$ result. The difference between our DARC $n = 2$ and the calculations of McLaughlin et al. (2011) are attributed to the fact that that our DARC $n = 2$ calculation was focused on generating accurate data only for fine-structure transitions within the ground term, while the results of McLaughlin et al. (2011) were focused on higher temperatures and higher n-shells in addition to the levels within the ground term. Again, our recommended collision strength is that produced by the DARC $n = 2$ calculation, based upon energy level, A-value comparisons with NIST data (Kramida et al. 2015) and published work, as discussed above.

The uncertainties in the DARC $n = 2$ results are again provided in a similar fashion using equation (3) and the standard deviation of the other BP and DARC models. Values for $\bar{x}_{\rm best}$ for Ne^{2+} are taken from the DARC $n = 2$, $n = 3$ and BP $n = 3$ calculations. Considering the effective collision strengths involving the higher excited state transitions (Figs 4 and 5), the DARC $n = 2$ model remains our recommended data set, with uncertainties given by the previously applied method. The uncertainty of the effective collision strengths from the DARC $n = 2$ calculations are 2–12 per cent (Fig. 3), 1–17 per cent (Fig. 4) and 2–12 per cent (Fig. 5).

To investigate the sensitivity of the results due to shifting our target energies to NIST values, we consider in Figs 6–8 the effect of these shifts on the collision strengths for the BP $n = 3$ Ne III calculation. The difference between the two BP calculations (with/without energy shift) is up to 89 per cent for the ($^3P_2$)–($^3P_1$) transition, up to 39 per cent for ($^3P_1$)–($^3P_0$) and up to 32 per cent for ($^3P_2$)–($^3P_0$). The large difference in the first transition is a result of the presence of near-threshold resonances. Thus, it is clearly important to include such shifts to NIST in the calculation of accurate low-temperature rate coefficients. For this reason, all of the data in our recommended data set, and the data used for the uncertainty estimates, include such NIST shifts. In general, any system that has near-threshold resonances would be particularly sensitive to such shifts, and this should be considered in future calculations of low-temperature fine-structure rate coefficients.

5 SUMMARY

We calculated collision strengths and effective collision strengths for Ne^+ and Ne^{2+} with BP and DARC R-matrix methods. We are interested in the rates at low temperatures (10–2000 K), so we focus on small energies (0.007–0.107 Ry for Ne^+ and 0.0058–0.1658 Ry for Ne^{2+}) and we perform small-scale R-matrix calculations. After comparing the energies, the Einstein A coefficient (A_{ij}), collision strengths (Ω_{ij}) and effective collision strengths (Υ_{ij}), we conclude that the DARC $n = 2$ model provides the most reliable collision strengths and effective collision strengths, with the Einstein A coefficients generated by this method being closest to the recommended values (i.e. NIST; Kramida et al. 2015). Further, effective collision strengths computed with the DARC $n = 2$ approach (Griffin et al. 2001; McLaughlin et al. 2011) result in rates that agree well

Table 5. Effective collision strengths Υ_{12} and the uncertainty %Δ for Ne II and Ne III ions calculated by the DARC approach using the $n = 2$ target expansion.

Temperature (K)	Ne II $2s^2 2p^5(^2P^0_{3/2})$–$(^2P^0_{1/2})$ Υ_{12}, %Δ	Ne III $2s^2 2p^4(^3P_2)$–$(^3P_1)$ Υ_{12}, %Δ	Ne III $2s^2 2p^4(^3P_2)$–$(^3P_0)$ Υ_{13}, %Δ	Ne III $2s^2 2p^4(^3P_1)$–$(^3P_0)$ Υ_{23}, %Δ
10	0.300, 13.99	0.633, 12.24	0.157, 11.26	0.186, 17.09
40	0.300, 13.74	0.635, 10.76	0.152, 8.50	0.184, 15.83
70	0.300, 13.74	0.636, 10.70	0.151, 8.03	0.183, 15.62
100	0.300, 13.74	0.639, 10.92	0.151, 7.88	0.182, 15.71
150	0.301, 13.82	0.644, 11.45	0.150, 7.63	0.181, 15.65
300	0.301, 13.69	0.640, 12.14	0.150, 7.63	0.177, 16.01
450	0.301, 13.69	0.627, 12.00	0.149, 6.54	0.174, 16.14
600	0.301, 13.57	0.615, 11.15	0.148, 4.46	0.172, 15.63
750	0.302, 13.67	0.604, 9.53	0.148, 2.23	0.169, 13.68
900	0.302, 13.52	0.597, 7.55	0.149, 2.59	0.167, 11.15
1050	0.302, 13.52	0.592, 5.38	0.150, 5.19	0.166, 8.53
1200	0.302, 13.52	0.591, 3.52	0.152, 7.62	0.165, 5.62
1350	0.302, 13.40	0.592, 2.23	0.155, 9.14	0.166, 3.35
1500	0.303, 13.50	0.596, 2.17	0.158, 10.32	0.167, 1.49
1650	0.303, 13.36	0.601, 2.88	0.162, 10.84	0.169, 1.28
1800	0.303, 13.36	0.607, 3.64	0.165, 11.40	0.171, 2.15
1950	0.303, 13.36	0.615, 4.28	0.169, 11.39	0.173, 3.30
2000	0.304, 13.46	0.617, 4.52	0.170, 11.53	0.174, 3.52

with the existing data at higher temperatures calculated by large-scale R-matrix methods.

ACKNOWLEDGEMENTS

This work was funded under NASA grant NASA-NNX15AE47G. BMMcL would like to thank Professors S. D. Loch and M. S. Pindzola and Auburn University for their hospitality during recent research visits.

REFERENCES

Abdel-Naby S. A., Ballance C. P., Lee T-G., Loch S. D., Pindzola M. S., 2013, Phys. Rev. A, 87, 022708
Abdel-Naby S. A., Pindzola M. S., Pearce A. J., Ballance C. P., Loch S. D., 2015, J. Phys. B: At. Mol. Opt. Phys., 48, 025203
Badnell N. R., 1986, J. Phys. B: At. Mol. Opt. Phys., 48, 025203
Berrington K. A., 1987, J. Phys. B: At. Mol. Phys., 20, 6379
Berrington K. A., Eissner W., Norrington P. H., 1995, Comput. Phys. Commun., 92, 290
Berrington K. A., Ballance C. P., Griffin D. C., Badnell N. R., 2005, J. Phys. B: At. Mol. Opt. Phys., 38, 1667
Burke P. G., 2011, R-Matrix Theory of Atomic Collisions: Application to Atomic, Molecular and Optical Processes. Springer-Verlag, New York
Butler K., Mendoza C., 1984, MNRAS, 208, P17
Chang J. J., 1975, J. Phys. B: At. Mol. Phys., 8, 2327
Colgan J., Loch S. D., Pindzola M. S., Ballance C. P., Griffin D. C., 2003, Phys. Rev. A., 68, 032712
Dyall K. G., Grant I. P., Johnson C. T., Plummer E. P., 1989, Comput. Phys. Commun., 55, 425
Eissner W., Martins P. de A. P., Nussbaumer H., Saraph H. E., Seaton M. J., 1969, MNRAS, 146, 63
Glassgold A. E., Najita J. R., Igea J., 2007, ApJ, 656, 515
Grant I. P., 2007, Quantum Theory of Atoms and Molecules: Theory and Computation. Springer-Verlag, New York, USA
Griffin D. C., Badnell N. R., Pindzola M. S., 1998, J. Phys. B: At. Mol. Phys., 31, 3713
Griffin D. C., Mitnik D. M., Badnell N. R., 2001, J. Phys. B: At. Mol. Opt. Phys., 34, 4401
Johnson C. T., Burke P. G., Kingston A. E., 1987, J. Phys. B: At. Mol. Phys., 20, 2553
Kramida A. E., Ralchenko Y., Reader J., NIST ASD Team, 2015, NIST Atomic Spectra Database (version 5.3), National Institute of Standards, Technology, Gaithersburg, MD. Available at: http://physics.nist.gov/asd
Ludlow J. A., Lee T-G., Ballance C. P., Loch S. D., Pindzola M. S., 2011, Phys. Rev. A., 84, 022701
Lykins M. L. et al., 2015, ApJ, 807, 118
McLaughlin B. M., Bell K. L., 2000, J. Phys. B: At. Mol. Opt. Phys., 33, 597
McLaughlin B. M., Daw A., Bell K. L., 2002, J. Phys. B: At. Mol. Opt. Phys., 35, 283
McLaughlin B. M., Lee T-G., Ludlow J. A., Landi E., Loch S. D., Pindzola M. S., Ballance C. P., 2011, J. Phys. B: At. Mol. Opt. Phys., 44, 175206
Malespin C., Ballance C. P., Pindzola M. S., Witthoeft M. C., Kallman T. R., Loch S. D., 2011, A&A, 526, A115
Meijerink R., Glassgold A. E., Najita J. R., 2008, ApJ, 676, 518
Munoz Burgos J. M., Loch S. D., Ballance C. P., Boivin R. F., 2009, A&A, 500, 1253
Norrington P. H., Grant I. P., 1981, J. Phys. B: At. Mol. Phys., 14, L261
Pradhan A. K., 1974, J. Phys. B: At. Mol. Phys., 7, L503
Saraph H. E., 1978, Comput. Phys. Commun., 15, 247
Saraph H. E., Tully J. A., 1994, A&AS, 107, 29
Schöier F. L., van der Tak F. F. S., van Dishoeck E. F., Black J. H., 2005, A&A, 432, 369
Seaton M. J., 1953, Proc. Roy. Soc. A, 218, 400
Witthoeft M. C., Whiteford A. D., Badnell N. R., 2007, J. Phys. B: At. Mol. Opt. Phys., 40, 2969
Wu D., Loch S. D., Pindzola M. S., Ballance C. P., 2012, Phys. Rev A., 85, 012711

SUPPORTING INFORMATION

Supplementary data are available at *MNRAS* online.

Please note: Oxford University Press is not responsible for the content or functionality of any supporting materials supplied by the authors. Any queries (other than missing material) should be directed to the corresponding author for the article.

This paper has been typeset from a TEX/LATEX file prepared by the author.